Chemical Physics Letters 568–569 (2013) 36–41

Contents lists available at SciVerse ScienceDirect

Chemical Physics Letters

journal homepage: www.elsevier.com/locate/cplett

Spectroscopic study on nonradiative transition and ionization of 5-methylpyrimidine at S_1 probed by the slow-electron velocity-map imaging (SEVI) technique

Jeongmook Lee, So-Yeon Kim, Sang Kyu Kim *

Department of Chemistry, KAIST, Daejeon 305-701, Republic of Korea

ARTICLE INFO

Article history:
Received 25 January 2013
In final form 28 February 2013
Available online 13 March 2013

ABSTRACT

Slow electron velocity-map imaging (SEVI) has been employed for the ionization spectroscopic study of the jet-cooled 5-methylpyrimidine in the first singlet $^1(n\pi^*)$ excited state. Resonant-enhanced two-color two-photon (1 + 1′) ionization spectrum gives well-resolved S_1 vibrational structures up to ~2400 cm^{-1} above the origin whereas spectral bands becomes completely broadened in the higher energy region as coupling of individual S_1 bands to dark states becomes significant. Ionization of the S_1 5-methylpyrimidine with different ionization wavelengths at several different delay times reveals the property of low-lying $^3(\pi\pi^*)$ triplet dark state which is prepared by fast nonadiabatic transition. SEVI spectra taken via various S_1 intermediate states provide the detailed vibrational structures of the 5-methylpyrimidine cation (D_0), also giving the adiabatic ionization energy of 9.1052 ± 0.0030 eV (73438 ± 24 cm^{-1}). Geometrical changes in the S_0–S_1–D_0 transitions are discussed from Franck-Condon simulations based on calculations by (time-dependent) density functional theory.

1. Introduction

Diaza-compounds such as pyrazine [1–3], pyrimidine [4–8], pyridazine [9–12], or their derivatives [13–17] have been both intensively and extensively studied for recent decades as ideal systems for investigation of nonadiabatic transition processes taking place among different electronic states. These also have been regarded as good model systems for studying excited-state dynamics of nuclear bases in DNA or RNA involved in energy relaxation mechanism as a self-protection process of living organisms from short wavelength radiation [18,19]. A number of spectroscopic and/or real-time dynamic studies in gas or condensed phase have been carried out for many molecular systems, revealing intimate interplays between nuclear motions and electronic configurations especially at critical points along the reaction pathway. Meanwhile, pyrimidine by itself got significant scientific interests as its intersystem crossing (ISC) process between S_1 and T_1 has been manifested clearly in a variety of spectroscopic studies. Effects of methylations or magnetic field have thus been systematically studied to unravel quantum nature of excited state mixing of pyrimidine compounds. The title molecule, 5-methylpyrimidine (5MP), in this regard, was also much studied. According to previous reported studies, ISC in 5MP becomes more facilitated compared to pyrimidine or 2-methylpyrimidine (2MP), whereas it is found to be less efficient than 4-methylpyrimidine (4MP) [14,15]. This is closely related to the extent of vibration/internal rotor coupling in S_1 which is directly correlated to the strength of S_1–T_1 coupling. Naturally, spectroscopic studies of methylated pyrimidine molecules have been mainly focused on the methyl rotor in terms of torsional barrier, density of states, and coupling to T_1 states [13–15].

In this Letter, we have carried out resonant-enhanced two-photon ionization spectroscopy of 5MP to provide the S_1–S_0 excitation spectrum up to ~2400 cm^{-1} above the origin. The S_1–T_1 intersystem crossing giving T_1 population in the microsecond time scale after the initial optical excitation is probed by the time-delayed photoelectron images. While most previous 5MP studies have been done with optical spectroscopy techniques such as laser induced fluorescence (LIF) spectroscopy [14,15], the photoelectron spectroscopy study of 5MP has been less investigated. Slow-electron velocity-map imaging (SEVI) technique [20,21] is thus employed to provide the detailed vibrational structure of the cation and the ionization potential of 5MP. The simulations based on calculations by density functional theory support experimental results.

2. Experiment

The experimental setup had been described in previous studies [22], and only a brief description is given here. The 5-methylpyrimidine sample (Aldrich, 96%) was heated to ~70 °C and seeded in the Ar carrier gas. The sample mixture was then expanded into vac-

* Corresponding author.
E-mail address: sangkyukim@kaist.ac.kr (S.K. Kim).

0009-2614/$ - see front matter © 2013 Elsevier B.V. All rights reserved.
http://dx.doi.org/10.1016/j.cplett.2013.02.074

uum through a nozzle orifice (Parker, General Valve series 9, 0.5 mm diameter) with a backing pressure ~2 bar before it was skimmed through a 0.5 mm diameter skimmer (Beam Dynamics). The excitation laser pulse (ω_1) in the 297–325 nm region was generated by frequency doubling of the dye laser output (Lumonics, Spectrummaster) pumped by the second harmonic output of Nd:YAG laser (Continuum, Powerlite). The ionization laser pulse (ω_2) was generated by frequency-doubling of the output of another dye laser (Lamda-Physik, Scanmate II) pumped by another Nd:YAG laser (Spectra-Physics, GCR-150). A wavemeter (Coherent, WaveMaster) was used for the wavelength calibration of two dye laser outputs. The two laser pulses were focused and overlapped by 250 mm focal length lenses onto the molecular beam in a counter-propagating manner. Photoelectrons were accelerated along the time-of-flight axis in the velocity mapping condition and projected onto a position-sensitive detector (Burle, 3040 FM CT, 40 mm diameter) coupled with a personal computer-interfaced CCD camera (Sony XC-ST50, 768 × 494 pixels) system in conjunction with the IMACQ Megapixel acquisition software [23]. The SEVI images were taken at low electric field condition (~44.3 V/cm), and reconstructed through the BASEX program [24].

Computationally, minimum energy structures and normal modes for ground state (S_0) and cationic state (D_0) of 5MP were calculated by density functional theory (DFT) method using the B3LYP function with a basis set of 6-311++(d,p). The first excited state (S_1) and triplet state (T_1) calculation was also performed employing time-dependent-DFT (TD-DFT) method with the same basis set. Franck-Condon analysis was carried out by using the Duschinsky transformation with a code developed by Peluso and co-workers [25–27]. All calculation were carried out with the GAUSSIAN09 set of program [28].

3. Results and discussion

Resonant-enhanced two-color two-photon (1 + 1′) ionization (R2PI) spectrum of 5MP is shown in Figure 1. The S_1–S_0 origin is found at 30 799 cm^{-1}, with a number of vibrational bands observed up to ~2400 cm^{-1} above the origin. Spectral features are very similar to those of laser-induced fluorescence (LIF) spectrum reported earlier by the Zwier group [14]. A broad diffuse background signal starts to appear at a few hundreds of cm^{-1} above the origin and persists at the higher internal energy, suggesting that coupling of S_1 to low-lying dark T_1 state is quite strong already at the low S_1 internal energy region. The S_1 band assignment based on TD-DFT using B3LYP with a basis set of 6-311++(d,p) seems to be quite appropriate as calculated values match well with experimental values (see Table 1). The band at 1024 cm^{-1} which had been tentatively assigned to 9a mode could be possibly due to another in-plane vibrational mode (*vide infra*). Fundamentals and combination bands of 6a, 1, and 12 are strongly observed in the S_1–S_0 excitation spectrum, and relative intensities are well reproduced by Franck-Condon analysis. Observed transitions and appropriate mode assignments are given in Table 2.

Evidence for the triplet population by ISC could be found by the delayed ionization method with different ionization wavelengths, as carried out by the Leutwyler group for 5-methyl-2-hydroxypyrimidine [16]. In Figure 2, the profiles of ion signal as a function of the delay time between the S_1–S_0 excitation laser pulse (ω_1) and D_0–S_1 ionization laser pulse (ω_2) are shown for different wavelengths of ω_2 at a fixed ω_1 wavelength. The excitation laser wavelength is fixed at the S_1–S_0 origin whereas three laser wavelengths of 230, 225, and 220 nm are used for ionization. The ion signal taken as a function of the ω_1–ω_2 delay time shows a peak with ~10 ns width corresponding to convolution of two laser pulses and a long tail at longer delay times. Interestingly, the ion signal intensity at longer delay times increases as the ω_2 wavelength becomes shorter. Considering the ionization potential (IP) of 73 438 ± 24 cm^{-1} for 5MP (*vide infra*), ionization with λ (ω_2) = 230, 225, or 220 nm gives the excess energy of 859, 1825, or 2835 cm^{-1}, above the adiabatic ionization threshold, respectively. Photoelectron images taken at λ (ω_2) = 220 nm show the change of vibrational characters of intermediate states with the change of the ω_1–ω_2 delay time. At $\Delta t = 0$ where the ion signal is maximized, the photoelectron image consists of distinct rings representing well-resolved vibrational states of the cation. On the

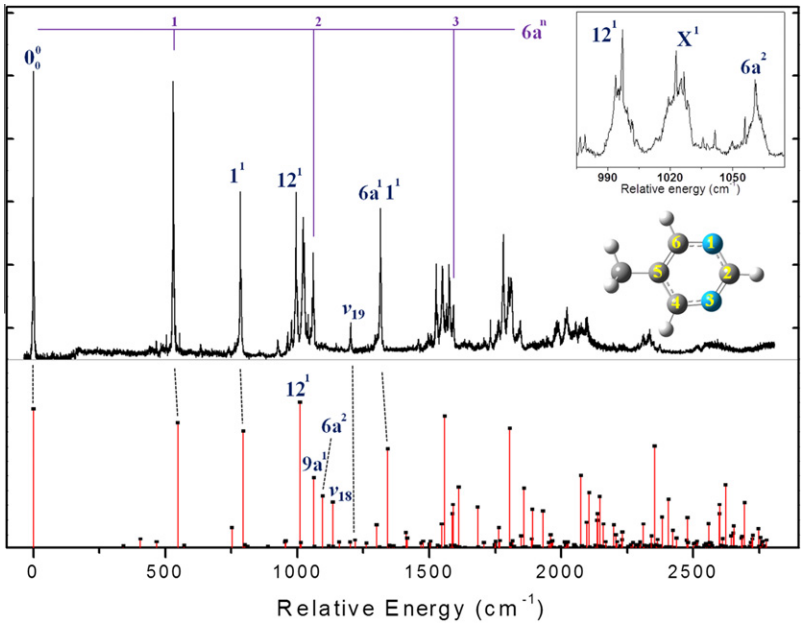

Figure 1. $S_1 \leftarrow S_0$ resonant-enhanced two-color (1 + 1′) ionization spectrum of 5-methylpyrimidine ionized at 218 nm (upper trace) and Franck-Condon simulation using unscaled DFT vibrational frequencies (lower trace). The spectral feature in range 980–1090 cm^{-1} is expanded and shown in the inset. The S_1 molecular structure of 5-methylpyrimidine is also shown with labels on atom.

Table 1
Experimental and calculated vibrational frequencies for the ground state, the first excited state, and the ionic ground state. All values are given cm^{-1}.

Mode	C_s [a]	S_1		Description[d]	C_{2v} [e]	D_0		S_0
		CAL[b]	EXP[c]			CAL[f]	EXP[c]	EXP[g]
ν_1	a″	129		CH_3 rotation	A_2	12		–
ν_2	a″	170		oop butterfly deformation	B_1	196		216
ν_3	a″	296		ring torsion (16a)	A_2	447		400
ν_4	a′	330		ip C–CH_3 bend	B_2	336		330
ν_5	a″	401		oop C_4–H bend (4)	B_1	587		728
ν_6	a′	406		ip (6b)	B_2	548		635
ν_7	a″	500		ring torsion+ oop s $C_{4,6}$–H bend (16b)	B_1	451		426
ν_8	a′	548	530	ip (6a)	A_1	549	536	558
ν_9	a″	566		oop as C–H(ring) bend	A_2	889		–
ν_{10}	a′	753		s N_1–C_2/C_4–C_5 stretch	B_2	1120		1163
ν_{11}	a″	783		oop C_6–H bend (5)	B_1	871		965
ν_{12}	a′	795	785	ip N_1–C–N_2 bend (1)	A_1	788	768	815
ν_{13}	a″	883		oop C_2–H bend	B_1	916		884
ν_{14}	a′	956		CH_3 rock	B_1	1053		1104
ν_{15}	a′	1011	997	ip C_3–C_4–C_5 bend (12)	A_1	998	978	1046
ν_{16}	a″	1052		CH_3 wag	B_2	992		989
ν_{17}	a′	1064	1023	ip C_6–H bend (9a)	A_1	1147	1112	1163
ν_{18}	a′	1136		s N_1–C_2/N_3–C_4 stretch + ip $C_{2,4}$–H bend (14)	B_2	1212		1197
ν_{19}	a′	1220	1203	C–CH_3 stretch	A_1	1240	1219	1242
ν_{20}	a′	1298		ip $C_{2,4,6}$–H bend	B_2	1320		1312
ν_{21}	a′	1313		ip (19a)	A_1	1469		1408
ν_{22}	a′	1379		ip (19b)	B_2	1415		1424
ν_{23}	a′	1411		CH_3 bend	A_1	1421		1392
ν_{24}	a″	1470		methyl C–H bend	B_2	1492		1455
ν_{25}	a′	1486		methyl C–H bend	B_1	1475		–
ν_{26}	a′	1502		as C_2–N_3/C_5–C_6 stretch (8a)	A_1	1603	1550	1582
ν_{27}	a′	1588		s C_2–N_3/C_5–C_6 stretch (8b)	B_2	1460		1563
ν_{28}	a′	3019		s methyl C–H stretch	A_1	3039		2863
ν_{29}	a″	3065		as methyl C–H stretch	B_2	3130		2980
ν_{30}	a′	3107		as methyl C–H stretch	B_1	3103		2940
ν_{31}	a′	3171		ip C_6–H stretch	B_2	3151		–
ν_{32}	a′	3217		ip C_2–H stretch	A_1	3250		3050
ν_{33}	a′	3240		ip C_4–H stretch	A_1	3150		3025

[a] The geometry of 5MP is distorted in plane of pyrimidine ring.
[b] DFT/B3LYP/6-311++(d,p) harmonic vibrational frequencies (unscaled).
[c] This letter.
[d] Description of normal-modes in S_1 state. ip, in-plane; oop, out-of-plane; s, symmetric; as, asymmetric. Corresponding Wilson's notations are denoted in parentheses.
[e] Neglecting the methyl group, C_{2v} symmetries apply to D_0 and S_0 states of 5MP. The correlation between the C_{2v} point group symmetry and the G_{12} symmetry group are $a_1 \leftrightarrow a_1'$, $a_2 \leftrightarrow a_2'$, $b_1 \leftrightarrow a_2''$, and $b_2 \leftrightarrow a_1''$.
[f] TD-DFT/B3LYP/6-311++(d,p) harmonic vibrational frequencies (unscaled).
[g] Taken from Ref. [29].

Table 2
Experimental vibrational frequencies and assignments for two-color (1 + 1′) R2PI spectrum of 5-methylpyrimidine. All values are given cm^{-1}.

Relative frequency (cm^{-1})		Assignment
0[a]		Origin
530	532[b]	$6a^1$
785	785[b]	1^1
997	997[b]	12^1
1023	1024[b]	X^1
1061	1061[b]	$6a^2$
1203		ν_{19}
1315		$6a^1 1^1$
1527		$6a^1 12^1$
1550		X^2
1576		1^2
1592		$6a^3$
1781		$1^1 12^1$
1810		$1^1 X^1$
1846		$1^1 6a^2$
1984		12^2
2121		$12^1 X^1$

[a] All frequencies are relative to S_1–S_0 origin at 30799 cm^{-1}.
[b] The frequencies are from Ref. [14].

other hand, photoelectron image shows diffuse features centered in the low kinetic-energy region when the delay time is shifted to 20 ns. This suggests that most of photoelectrons at $\Delta t = 20$ ns are associated with highly vibrationally excited cationic states, indicating that the optically pumped S_1 state has been transformed to vibrationally hot states in the low-lying electronic state. Since the rate of ISC is around $\sim 10^7\ s^{-1}$ for 5MP, it is quite reasonable to conclude that the origin of long-tail ion signal should be ascribed to the ionization from the low-lying triplet T_1 state ($^3\pi\pi^*$) which is calculated to be $\sim$2900 cm^{-1} below the S_1 state. The role of T_2 ($^3n\pi^*$) in ISC had been emphasized in some previous reports, and this needs to be further investigated [30,31].

For estimation of the ionization potential of 5MP, photoelectron images are taken at a number of different ionization wavelengths whereas the excitation wavelength is fixed for the S_1–S_0 origin at 30799 cm^{-1}. The peak position of the outmost ring associated with the D_0–S_1 origin transition is plotted versus the ionization wavelength, giving a linear relationship with respect to each other, Figure 3. Extrapolation of the linear fit to the center of the image corresponding to the zero-kinetic energy gives rise to the adiabatic ionization potential, which is estimated to be 73438 ± 24 cm^{-1} (9.1052 ± 0.0030 eV), after correction for the field effect which is proportional to $\sim 6\sqrt{F}$. This value is $\sim$0.1903 eV higher than IP of 8.9149 eV predicted by density functional theory (DFT) calculation with the B3LYP/6-311++(d,p) level.

SEVI spectra taken via various S_1 intermediate states are shown in Figure 4. These spectra provide complete vibrational structure of the 5MP cation up to $\sim$2800 cm^{-1} above the D_0 origin. Since the

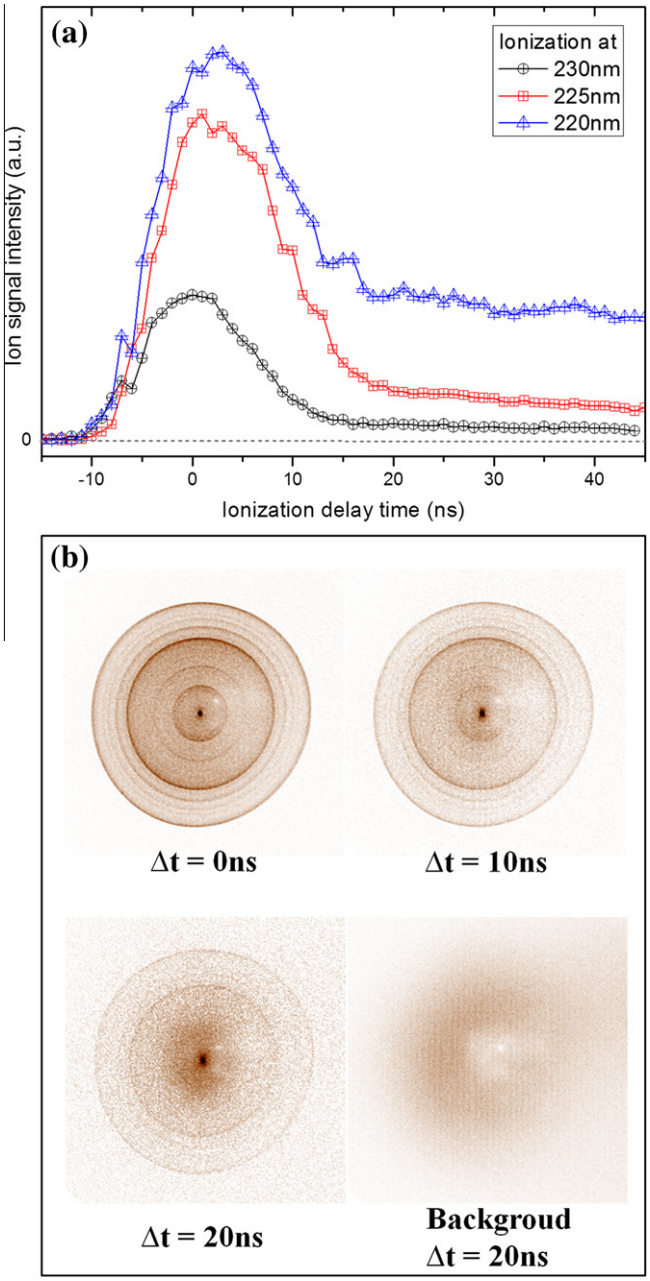

Figure 2. (a) Profiles of ion signal with varying the delay time between excitation and ionization laser pulses at ionization wavelengths of 230, 225, and 220 nm via the S_1–S_0 origin of 5MP. (b) The $(1 + 1')$ photoelectron images taken at the ionization wavelength of 220 nm with three different delay times are shown. All images are background-subtracted.

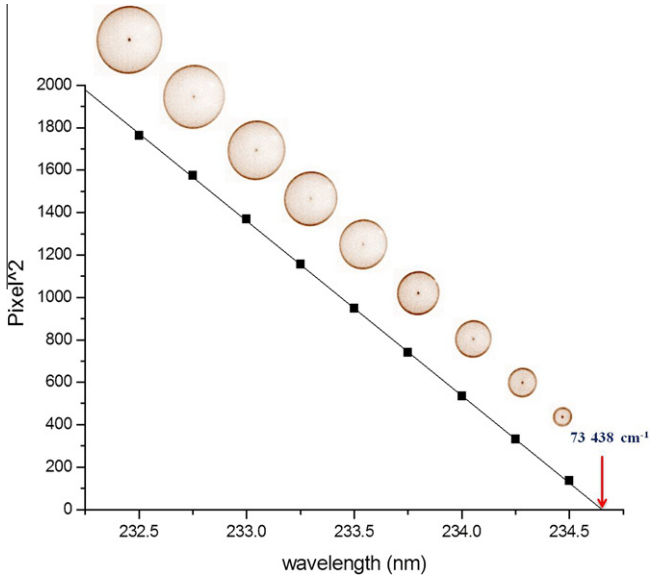

Figure 3. Photoelectron kinetic energies associated with the D_0 zero-point energy level are plotted versus the varying ionization wavelength at the fixed excitation energy at the S_1–S_0 origin transition. Several photoelectron images are shown together. The IP from the extrapolation is denoted by an arrow.

vibrational mode assignment is more straightforward for the cationic ground state, the S_1 mode assignment using SEVI spectra based on the propensity rule of $\Delta v = 0$ turns out to be quite useful. All vibration bands observed in SEVI spectra are assigned and given in Table 3. The SEVI spectrum taken via the S_1 origin shows strong activation of in-plane symmetric modes and it is in good agreement with D_0–S_1 Franck-Condon simulation from DFT vibrational frequencies listed in Table 1. It is noteworthy that the $8a^+$ mode at 1550 cm^{-1} is observed as intense as the D_0–S_1 origin band. The $8a^+$ mode corresponds to in-plane symmetric ring-distortion, reflecting a drastic geometrical change of 5MP upon ionization in terms of the NCN internal angle of the pyrimidine moiety. Minimum energy geometrical parameters of 5MP at the ground (S_0), first electronically excited (S_1), and ionic ground (D_0) states are listed in Table 4. Geometrical changes in terms of the ring distortion are significant for both S_1–S_0 and D_0–S_1 transitions. It is quite noteworthy though that the S_1 minimum structure converges at the C_S geometry whereas the structure converges to C_{2V} for the D_0 minimum energy. Upon the D_0–S_1 ionization, the bond lengths of N_1–C_6 and N_3–C_4 are shortened about 0.05 Å whereas the N_1–C_2–N_2 bond angle becomes ~3.5° smaller. This geometrical change matches quite well with nuclear displacement vectors of the $8a^+$ normal mode which may be represented as N_1–C_6 /N_3–C_4 symmetric stretching, and accordingly $8a^+$ mode and its combination bands are found to be strongly activated in all SEVI spectra taken in this Letter. It is interesting to note that strong $8a^+$ combination bands via all S_1 vibrations are observed for 5-MP, while strong $8a^+$ mode via only S_1 origin and weak $8a^+$ mode via S_1 1^1 and $16a^4$ been observed in the D_0–S_1 ionization for pyrimidine [32,33].

Other normal modes of $6a^+$, 1^+, and $9a^+$ are found to be also strongly activated in the SEVI spectrum taken via S_1 origin. Franck-Condon analysis based on DFT calculations reproduces the SEVI spectrum very well, giving appropriate vibrational mode assignments for the 5MP cation in the ground state with accurate frequency values. Analyses of other SEVI spectra via various S_1 intermediate states are quite straightforward as the propensity rule seems to be kept well in the D_0–S_1 ionization process. Consequently, S_1 mode assignments for 6a, 1, 12, and $6a^2$ are consistent with those reported earlier by the Zwier group [14] whereas a weakly observed 1200 cm^{-1} band is newly assigned to the C–CH_3 stretching mode (ν_{19}). The SEVI spectrum taken via the 1023 cm^{-1} S_1 band, however, shows somewhat complicated spectral feature. This band had been tentatively assigned to 9a mode in Ref. [14]. And yet, the $9a^+$ mode at 1112 cm^{-1} is found to be only weakly activated whereas 12^+ and a new band at 1029 cm^{-1} are more strongly observed. This SEVI spectral pattern suggests that the 1023 cm^{-1} S_1 band could represent a mixed (unknown) X mode resulting from Fermi-resonance type interactions. Three vibration bands of 12, X, and $6a^2$ in the S_1–S_0 R2PI spectrum over the 980–1090 cm^{-1} region (Figure 1) show quite congested and broadened spectral features indeed, implying of strong couplings among optically bright and dark states [14].

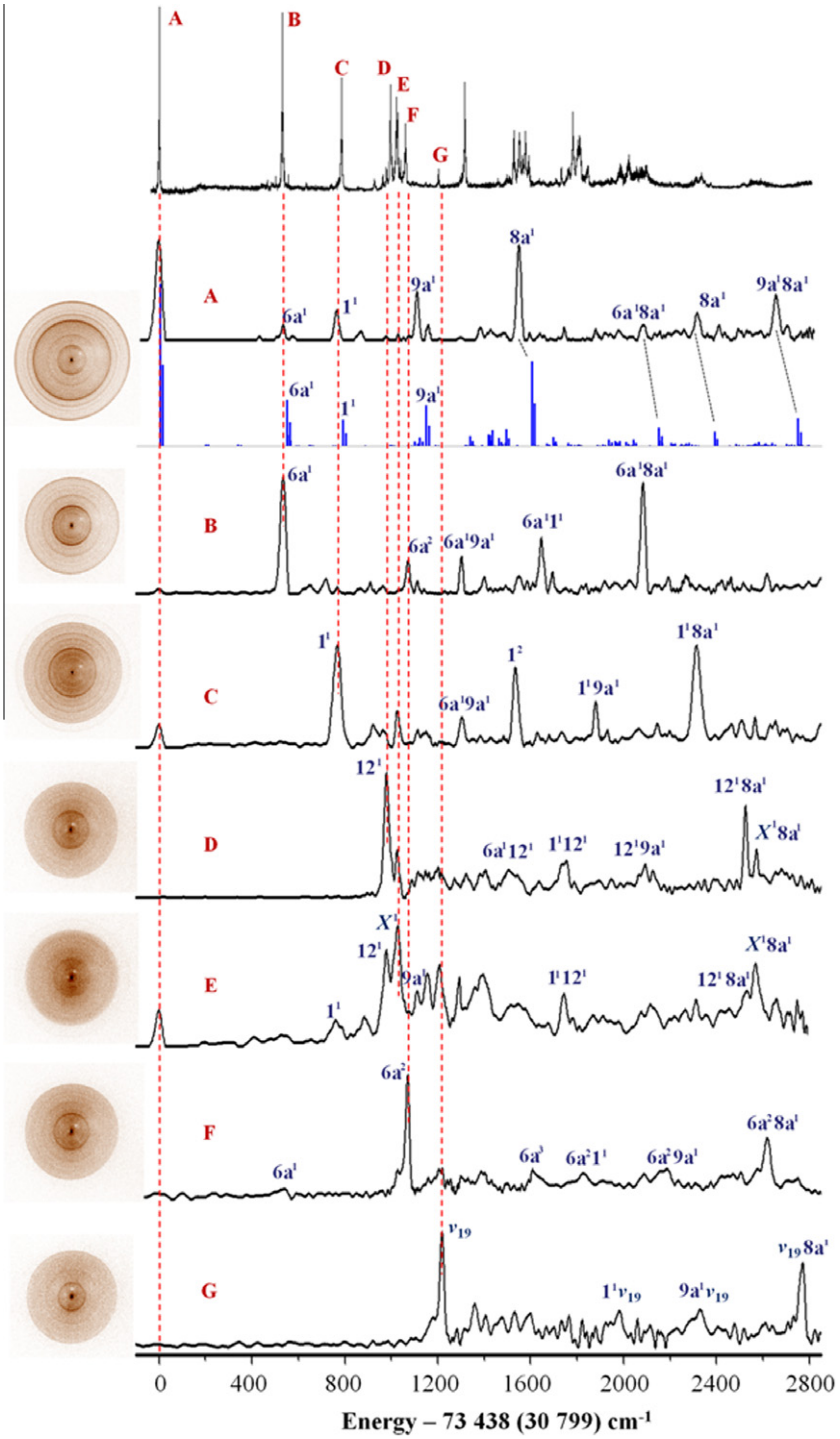

Figure 4. SEVI images and spectra of 5MP taken via various intermediate states are shown. The S_1 vibronic states labeled with A, B, C, D, E, F, and G in the R2PI spectrum are used as intermediate states for (1 + 1′) SEVI processes. Franck-Condon simulation using the DFT vibrational frequencies is shown for comparison (blue sticks) (For interpretation of the references to color in this figure legend, the reader is referred to the web version of this article.).

4. Conclusions

Nonradiative transition and ionization of 5-methylpyrimidine has been spectroscopically studied using SEVI and R2PI methods. Photoelectron images taken as a function of the ω_1–ω_2 delay time confirm that the optically pumped S_1 state has been transformed to the low-lying triplet T_1 state ($^3n\pi^*$) which is calculated to be $\sim$2900 cm^{-1} below the S_1 ($^1n\pi^*$) state. The clear observation of the drastic time-dependence of the photoelectron image is consistent with the rather slow intersystem crossing rate ($\tau_{ISC} \sim 0.1$ μs) of the title molecule. Extrapolation of the linear fit to the change of photoelectron kinetic energy versus ionization wavelength gives the adiabatic ionization potential of 9.1052 ± 0.0030 eV (73 438 ± 24 cm^{-1}) for 5MP. The SEVI spectra taken via various S_1 intermediate states provide accurate vibrational frequencies of the 5MP cationic ground state. The $8a^+$ mode associated with in-plane ring distortion is significantly activated in the D_0–S_1 ionization, suggesting of the drastic geometrical change as the electron is

Table 3
All vibrations denoted in SEVI spectra in Figure 4. All values are given cm^{-1}.

Assignment	Selected S_1 intermediate state						
	0^0	$6a^1$	1^1	12^1	X^1	$6a^2$	v_{19}
0^0	0	0	0		0		
$6a^1$	536	536				541	
1^1	765		769		761		
12^1				979	978		
X^1			1025	1025	1029	1027	
$6a^2$		1073				1071	
$9a^1$	1112				1111		
v_{19}							1219
$6a^19a^1$		1302	1304				
$6a^112^1$				1505			
1^2			1534				
$8a^1$	1550						
$6a^3$						1608	
$6a^11^1$		1646					
1^112^1				1753	1743		
$6a^21^1$						1826	
1^19a^1			1880				
1^1v_{19}							1983
$6a^18a^1$	2085	2083					
12^19a^1				2093			
$6a^29a^1$						2187	
1^18a^1	2316		2314				
$9a^1v_{19}$							2330
12^18a^1				2524	2532		
X^18a^1				2573	2568	2578	
$6a^28a^1$						2618	
$9a^18a^1$	2656						
$v_{19}8a^1$							2771

Table 4
Geometry of 5-methylpyrimidine in the ground, first excited and ionic ground states. See Figure 1 for labeling of atoms. Bond lengths in Angström and angles in degrees.

	S_0	S_1	D_0
$r(N_1–C_6)$	1.3354	1.3774	1.3165
$r(N_3–C_4)$	1.3353	1.3661	1.3164
$r(N_1–C_2)$	1.3344	1.3524	1.3243
$r(N_3–C_2)$	1.3345	1.2935	1.3244
$r(C_5–C_6)$	1.3960	1.3733	1.4073
$r(C_5–C_4)$	1.3961	1.4315	1.4073
$a(C_2–N_1–C_6)$	116.09	120.00	125.89
$a(C_2–N_3–C_4)$	116.09	127.92	125.89
$a(N_1–C_6–C_5)$	123.20	123.11	121.26
$a(N_3–C_4–C_5)$	123.20	116.12	121.26
$a(C_4–C_5–C_6)$	114.88	115.78	112.20
$a(N_1–C_2–N_2)$	126.52	117.08	113.50

being removed. The S_1 vibronic mode assignment has been either confirmed or newly done based on the propensity rule kept in the D_0–S_1 ionization. Spectral congestion and broadening in the S_1–S_0 transition process suggests that vibronic couplings among optically bright and/or dark states are quite active.

Acknowledgements

This letter was supported by the National Research Foundation (2012-0005607) and by the WCU program (R31-10071). The support from the center for Space-time Molecular Dynamics (2012-0000779) is also appreciated.

Appendix A. Supplementary data

Supplementary data associated with this article can be found, in the online version, at http://dx.doi.org/10.1016/j.cplett.2013.02.074.

References

[1] J. Kornrnandeur, W. Majewski, W. Meerts, D. Pratt, Annu. Rev. Phys. Chem. 38 (1987) 433.
[2] L.A. Miller, J.R. Barker, J. Chem. Phys. 105 (1996) 1383.
[3] M. Tsubouchi, B.J. Whitaker, T. Suzuki, J. Phys. Chem. A 108 (2004) 6823.
[4] I. Yamazaki, M. Fujita, H. Baba, Chem. Phys. Lett. 57 (1981) 431.
[5] A.K. Jameson, E.C. Lin, Chem. Phys. Lett. 79 (1981) 326.
[6] T.G. Dletz, M.A. Duncan, A.C. Pulu, R.E. Smalley, J. Phys. Chem. 86 (1982) 4026.
[7] Y. Matsumoto, L.H. Spangler, D.W. Pratt, Chem. Phys. Lett. 98 (1983) 333.
[8] J.A. Konings, W.A. Majewski, Y. Matsumoto, D.W. Pratt, W.L. Meerts, J. Chem. Phys. 89 (1988) 1813.
[9] M. Terazima, S. Yamaguchi, N. Hirota, O. Kitao, H. Nakatsuji, Chem. Phys. 107 (1986) 81.
[10] Y. Masumoto, S.K. Kim, T. Suzuki, J. Chem. Phys. 119 (2003) 300.
[11] K.-W. Choi et al., Chem. Phys. Chem. 5 (2004) 737.
[12] D.-S. Ahn et al., Chem. Phys. Chem. 9 (2008) 1610.
[13] K. Uchida, I. Yamazaki, H. Baba, Chem. Phys. 35 (1978) 91.
[14] R.E. Bandy, J. Nash, T.S. Zwier, J. Chem. Phys. 95 (1991) 2317.
[15] L. Alvarez-Valtierra, X.-Q. Tan, D.W. Pratt, J. Phys. Chem. A 111 (2007) 12802.
[16] S. Lobsiger, H.-M. Frey, S. Leutwyler, Phys. Chem. Chem. Phys. 12 (2010) 5032.
[17] Y. He, C. Wu, W. Kong, Chem. Phys. Lett. 391 (2004) 38.
[18] B.B. Brady, L.A. Peteanu, D.H. Levy, Chem. Phys. Lett. 147 (1988) 538.
[19] S. Ullrich, T. Schultz, M.Z. Zgierski, A. Stolow, Phys. Chem. Chem. Phys. 6 (2004) 2796.
[20] A. Osterwalder, M.J. Nee, J. Zhou, D.M. Neumark, J. Chem. Phys. 121 (2001) 6317.
[21] D.M. Neumark, J. Phys. Chem. A 112 (2008) 13287.
[22] D.-S. Ahn, J. Lee, Y.C. Park, Y.S. Lee, S.K. Kim, J. Chem. Phys. 136 (2012) 024306.
[23] W. Li, S.D. Chambreau, S.A. Lahankar, A.G. Suits, Rev. Sci. Instrum. 76 (2005) 063106.
[24] V. Dribinski, A. Ossadtchi, V.A. Mandelshtam, H. Reisler, Rev. Sci. Instrum. 73 (2002) 2634.
[25] F. Duschinsky, Acta Physicochim. URSS 7 (1937) 551.
[26] A. Peluso, F. Santoro, G.D. Re, Int. J. Quantum Chem. 63 (1997) 233.
[27] R. Borrelli, A. Peluso, J. Chem. Phys. 119 (2003) 8437.
[28] M.J. Frisch et al., Gaussian 09, Revision A.1, Gaussian, Inc., Wallingford, CT, 2009.
[29] S.B. Kartha, Spectrochm. Acta A 38 (1982) 859.
[30] M.A. El-Sayed, J. Chem. Phys. 18 (1963) 2834.
[31] M. Baba, J. Phys. Chem. A 115 (2011) 9514.
[32] S. Sato, K. Omiya, K. Kimura, J. Electron Spectrosc. Relat. Phenom. 97 (1998) 121.
[33] M. Riese, J. Grotemeyer, Anal. Bioanal. Chem. 386 (2006) 59.